Gated Luminescence Imaging of Silicon Nanoparticles

Jinmyoung Joo[†], **Xiangyou Liu**[‡], **Venkata Ramana Kotamraju**[‡], **Erkki Ruoslahti**[‡,§], **Yoonkey Nam**[‖], and **Michael J. Sailor**[*,†]

[†]Department of Chemistry and Biochemistry, University of California, San Diego, 9500 Gilman Drive, mc 0358, La Jolla, California 92093, United States

[‡]Cancer Research Center, Sanford-Burnham Medical Research Institute, La Jolla, California 92037, United States

[§]Center for Nanomedicine and Department of Cell, Molecular and Developmental Biology, University of California, Santa Barbara, Santa Barbara, California 93106-9610, United States

[‖]Department of Bio and Brain Engineering, Korea Advanced Institute of Science and Technology (KAIST), Daejeon 305-701, Korea

Abstract

The luminescence lifetime of nanocrystalline silicon is typically on the order of microseconds, significantly longer than the nanosecond lifetimes exhibited by fluorescent molecules naturally present in cells and tissues. Time-gated imaging, where the image is acquired at a time after termination of an excitation pulse, allows discrimination of a silicon nanoparticle probe from these endogenous signals. Because of the microsecond time scale for silicon emission, time-gated imaging is relatively simple to implement for this biocompatible and nontoxic probe. Here a time-gated system with ~10 ns resolution is described, using an intensified CCD camera and pulsed LED or laser excitation sources. The method is demonstrated by tracking the fate of mesoporous silicon nanoparticles containing the tumor-targeting peptide iRGD, administered by retro-orbital injection into live mice. Imaging of such systemically administered nanoparticles *in vivo* is particularly challenging because of the low concentration of probe in the targeted tissues and relatively high background signals from tissue autofluorescence. Contrast improvements of >100-fold (relative to steady-state imaging) is demonstrated in the targeted tissues.

Continuous wave imaging | Time-gated imaging
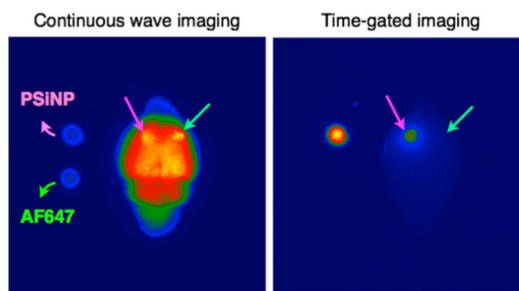
Keywords

time-gated luminescence imaging; bioimaging; intravital imaging; targeting peptides; tumor; cancer; *in vivo* imaging; iRGD; porous silicon

Fluorescence imaging is one of the most versatile tools in biomedical research and clinical diagnostics.[1,2] The method commonly employs an exogenous fluorescent probe, and a major limitation is the substantial background signal originating from tissue autofluorescence, which interferes with and limits the discrimination of the probe from tissues. Several approaches to mitigate this issue have been pursued, including use of fluorophores that emit in the near-infrared (NIR) range where tissue autofluorescence levels are lower,[3–6] two-photon or upconverting probes that harness NIR excitation sources which do not excite tissue fluorophores,[7–10] and longer-lived probes (lanthanides,[11–13] transition metal bipyridine complexes,[14,15] quantum dots[16,17]) imaged by time-gated luminescence.[18–20] This latter method employs a pulse of excitation and captures the emitted light at a delayed time in order to eliminate short-lived signals associated with tissue autofluorescence. A class of luminescent imaging probes based on silicon quantum dots[21–37] has gained much recent attention due to their significantly lower toxicity relative to quantum dots derived from heavy metals such as cadmium,[22,38] their increased photostability relative to conventional organic fluorophores,[39,40] their emission in the NIR, tissue-penetrating region of the spectrum, their biodegradability, and their compatibility with living systems.[32] Because of the indirect nature of the silicon band gap,[41] silicon quantum dots display a very long radiative lifetime (>10 μs), and this has been harnessed for time-gated imaging, allowing significant improvement in discrimination from interfering tissue autofluorescence in animal images.[24] A porous form of silicon quantum dots can be prepared in an electrochemical process by etching of silicon wafers, and these porous silicon nano-particles (PSiNPs) have shown good biocompatibility and biodegradability *in vivo*.[24,32] The porous formulation also provides increased functionality by allowing the incorporation of a range of therapeutic molecules,[32,42–44] MRI contrast agents,[45,46] or additional imaging probes.[32,47–49]

In the first report of time-gated luminescence imaging using PSiNPs, we used a commercial animal imaging system that was limited to relatively short delay times (<25 ns) due to the fixed repetition rate of the pulsed laser.[24] The improvement in signal-to-noise ratio in imaging PSiNPs against various tissue backgrounds was relatively modest due to this limitation, and much lower than the theoretical prediction. Here we present a system specifically designed to capitalize on the microsecond time domain of PSiNP emission,

using nanosecond-range pulsed laser or LED sources and a commercial intensified CCD camera that can be gated from off to on within 10 ns. We refer to this method as gated luminescence imaging of silicon nanoparticles (GLISiN) and demonstrate its utility in imaging of IV-administered PSiNPs. Unlike the previous PSiNPs used in luminescence imaging, the PSiNPs used in this study are modified with tumor-targeting peptides, and we show that the optimized system yields contrast improvements of >100× when tracking the *in vivo* fate of the targeted nanoparticles relative to steady-state imaging.

RESULTS AND DISCUSSION

The imaging system for GLISiN (Figure 1a) is similar to those previously described in the literature for imaging of long-lived transition metal complexes[14] involving pulsed excitation from a laser or LED and a time-gated CCD camera programmed to acquire the image beginning at a fixed time after the excitation source is turned off. The time-gated camera used in the present studies was an intensified CCD camera (ANDOR iStar), which is gated "on" by application of high voltage to the intensifier screen. The gating pulses used to acquire images are given schematically in Figure 1b. For LED illumination, an external pulse generator (model 3390, Keithley Instruments Inc.) simultaneously applied voltage to a UV LED and TTL pulse to trigger the camera, which was programmed to energize the intensifier after the appropriate time delay (Figure 1b, "gated"). For laser excitation, a tripled YAG-pumped optical parametric oscillator (Opolette 355, Opotek Inc.) was used in place of the LED, and the CCD camera was triggered by TTL pulse from the internal pulse generator of the laser. For continuous wave imaging (CWI), the camera intensifier was triggered with no preprogrammed delay such that it became active simultaneously with the excitation light pulse (Figure 1b, CW).

We first tested the ability of the time-gated GLISiN method to separate the long-lived photoluminescence signal of PSiNPs from the short-lived (nanosecond) fluorescence signals of a conventional fluorophore and tissue autofluorescence in *ex vivo* tissue samples. Luminescent PSiNPs were prepared with a Si-SiO$_2$ core—shell structure as described previously[50,51] and polyethylene glycol (PEG) was grafted to the outer shell to improve colloidal stability and biocompatibility. We chose a mouse brain for this set of experiments (Figure 1c) due to the typically high levels of autofluorescence seen from these tissues. A UV LED (365 nm) was used as excitation source. Under steady-state conditions, the autofluorescence signal from the mouse brain was much stronger than the signal from phantoms consisting of small spots of PSiNPs or the molecular dye Alexa Fluor 647 (AF647), Figure 1e. The quantity of PSiNPs (150 ng) and AF647 (2.5 ng) used in each of the phantoms was chosen to yield comparable photoluminescence intensity in the steady-state images. The excited state of the PSiNPs used in this study decays with a half-life of 60 μs, significantly longer than the (<10 ns) lifetime of organic dyes (rhodamine, fluorescein, Alexafluor) or tissue autofluorescence signals (Supporting Information Figures S1 and S2). When excited with pulsed excitation from the same LED (pulse duration 500 μs, repetition rate 10 Hz) and observed 5 μs after termination of the excitation pulse, the tissue autofluorescence and AF647 were eliminated while the PSiNPs still displayed bright emission (Figure 1f,g).

We next investigated the ability of GLISiN to identify Si nanoparticles in *ex vivo* tissue samples. The major organs and tumor were harvested from a BALB/c mouse containing a xenografted 4T1 breast tumor and arrayed on an imaging table, with each organ placed adjacent to small phantom sample spots of PSiNPs and AF647. The static (CW) photoluminescence images (Figure 2a) showed signals from all the organs, with the brain, liver, kidney, lung, and tumor showing particularly strong tissue autofluorescence. The images of the PSiNP and AF647 phantoms were relatively weak in these images, displaying intensity roughly comparable to the auto-fluorescence from the heart and spleen. Small quantities of PSiNPs and AF647 were then directly injected in separate locations in each of the mouse tissues. The CW photoluminescence images obtained at this point (Figure 2b) were similar to the corresponding images in Figure 2a; the strong tissue autofluorescence background from the organs made it difficult to discern the luminescence signal from either imaging probe, although the regions of injection were slightly brighter in some tissues (brain, liver, spleen, tumor). For instance, the signal-to-noise ratio (SNR) for the injected region relative to neighboring tissue area in the brain was less than 1 for both PSiNPs and AF647, which is not distinguishable from background (Supporting Information Figure S3, Table S1, and Note S1). The time-gated (GLISiN) photoluminescence images (Figure 2c,d) showed remarkably enhanced signals from the PSiNP phantoms and PSiNP-injected regions, whereas AF647 and the native tissues were essentially undetectable. The SNR of the PSiNP-injected region of the brain shows enhancement of 50— 100-fold relative to the CW images (Supporting Information Table S1). To confirm this persistent signal at the injection site arose from PSiNPs, we measured photoluminescence decays at each region (Figure 2e). The PSiNP-injected tissue regions show a prompt decay component due to the short-lived tissue autofluorescence and a longer component corresponding to the ~60 μs half-life of PSiNPs. This long-lived signal is readily distinguished from tissue autofluorescence in the time domain, and the GLISiN images could separate PSiNPs from endogenous fluorescence signals with high fidelity regardless of tissue type (Figure 2d and Supporting Information Table S2).

It should be pointed out that all the images presented in this work do not employ intensity thresholding or selected area images to identify the PSiNP probe. In conventional fluorescence imaging methods, these approaches, along with the use of low energy excitation and long pass filter sets, are often used to reduce unwanted tissue autofluorescence. The GLISiN method yields superior SNR even with short wavelength (365 nm) excitation and relatively short wavelength (460 nm long-pass filter) observation (Supporting Information Figure S4 and Table S3).

Finally, we investigated the ability of GLISiN to identify Si nanoparticles that have been introduced to systemic circulation in live animals and targeted to tumors. As with the above *in vitro* experiments, the luminescent PSiNPs were prepared with a Si–SiO$_2$ core–shell structure and a PEG coating, but the tumor-homing peptide iRGD was attached to the distal end of the grafted PEG chains. The cyclic peptide iRGD has a three-phase mode of action of (1) binding to alpha-v integrins on tumor endothelium via the RGD moiety, (2) undergoing a proteolytic cleavage to expose a binding motif for neuropilin-1, and then (3) harnessing the neuropilin-1-dependent transport pathway to mediate penetration of the peptide–nanoparticle construct into tissue and cells.[52,53] Imaging of such systemically administered

nanoparticles is typically limited by low accumulation of probe in the targeted tissues and relatively high background signals from the tissues of interest. The problem is confounded by the high variability of autofluorescence intensity and wavelength in different tissue types and even within the same tissues,[54,55] as is evident in the CW images of tissues presented above. In addition, irregularly arranged tissue structures lead to heterogeneous scattering in CW optical images that can be reduced somewhat in time-gated images.[56] We hypothesized that the GLISiN method would improve our ability to identify and quantify specific accumulation of the actively targeted nanoparticles.

PSiNP conjugated to iRGD (PSiNP–iRGD) and control PSiNPs were administered through retro-orbital injection of mice bearing 4T1 breast tumors. An additional mouse bearing a 4T1 breast tumor was used as a PBS-injected control. No overt signs of distress or morbidity were observed in the mice injected with PSiNP or PSiNP–iRGD formulations. After 4 h of circulation, the mice were sacrificed and the major organs were harvested. Fluorescence images of the organs, acquired using a conventional animal imaging system (IVIS 200, Xenogen), showed slightly more intense signals in the tumors of the mice injected with control PSiNP and PSiNP–iRGD constructs than in the PBS-injected mouse (Figure 3a and Supporting Information Figure S5). The observed apparent accumulation of the control PSiNPs in the tumor could be attributed to the enhanced permeability and retention (EPR) effect that is often exhibited by longer-circulating nanoparticles.[32,57] However, as will be discussed below, the GLISiN images rule out the presence of significant non-targeted PSiNPs in the tumor. The greater degree of accumulation seen with the PSiNP–iRGD formulation is consistent with the previously observed ability of the iRGD peptide to target and deliver nanoparticles to this tumor type.[58]

Consistent with the IVIS images, luminescence images obtained in the CW mode showed higher SNR in the tumor of the PSiNP–iRGD-injected mice (8.7) than that of the mice injected with nontargeted PSiNPs (3.7) (Figure 3b and Supporting Information Figure S6). Although use of a long-pass emission filter reduced the intensity of the tissue autofluorescence signal, it still interfered with the luminescence signal from the PSiNPs somewhat,[59] and CW images of the organs displayed significant signals even from the PBS-injected control animal, making it difficult to distinguish the PSiNPs from tissue autofluorescence. By contrast, the time-gated GLISiN images suppressed tissue autofluorescence signals significantly (Figure 3c,d), increasing the SNR from the tumor in the PSiNP–iRGD-injected animal from 8.7 in the CW image to 51.2 in the GLISiN image. Although the IVIS, CW, and GLISiN images show similar trends in biodistribution of the nanoparticles, the images obtained with IVIS and CW modes show substantially inferior SNR (Figure 3e). In particular, the GLISiN image definitively shows that the somewhat larger steady-state signal seen in the control animal injected with nontargeted PSiNPs does not necessarily derive from PSiNPs; rather, it could be a result of animal-to-animal variability in the autofluores-cent background from the tumors (Supporting Information Figure S7). Furthermore, based solely on the CWI and IVIS images, one could conclude that passive accumulation of nontargeted PSiNPs to the tumor is almost half as effective as active accumulation of iRGD-targeted PSiNPs. However, the GLISiN data show that passive accumulation of the nanoparticles was only one-tenth as effective as active targeting of the iRGD-conjugated nanoparticles in that set of animals (Supporting Information Figure S6).

Because it harnesses the intrinsic luminescence of the silicon nanoparticle, the GLISiN method affords signals that are more directly attributable to the nano-particle, allowing a more reliable assessment of nano-particle biodistribution. Fluorescent labels can become detached from a nanoparticle host during circulation, making it more difficult to track particle vs label. In addition, small differences in surface chemistry can influence *in vivo* fate in unpredictable ways. For example, in the present set of experiments, the actively targeted PSiNP–iRGD formulation showed greater uptake in the spleen relative to passively targeted PSiNPs ($p < 0.05$, Supporting Information Figure S8), and some animals showed higher accumulation of passively targeted PSiNPs in the lungs relative to actively targeted PSiNP–iRGD. Lung accumulation of PSiNPs was quite variable from animal to animal and not statistically significant relative to PSiNP iRGD accumulation ($p > 0.1$). The most statistically significant difference in the specificity of actively targeted PSiNP–iRGD relative to passively targeted PSiNP was seen in the tumors ($p < 0.005$).

CONCLUSION

By involving time-gated imaging of the relatively long-lived excited state of silicon nanoparticles, the GLISiN method provides a robust means to eliminate tissue autofluorescence and to distinguish the nano-particle from other exogenous fluorescent probes. In this study, we focused on the use of an LED illumination source in order to demonstrate a relatively low-cost system. However, LED sources are limited by slow turn-off times, which require a longer gate delay and reduce the magnitude of the signal that can be accumulated during the gate window period. Accordingly, the SNR of the method can be significantly increased using pulsed laser excitation (Figure 3d,e). As a targeted system, PSiNPs provide a promising model system due to their larger size (100–200 nm), which allows the attachment of multiple targeting probes to enable multivalency[60] and a large inner pore volume to accommodate therapeutics.[42,47,61] In addition, the use of two-photon excitation may further expand the utility of the method (including deeper tissue penetration), as PSiNPs are known to be excitable in a two-photon mode.[32,62] In addition to their ability to provide high contrast images by time-gating, the biocompatibility and biodegradable characteristics of PSiNPs overcomes the safety issues of cytotoxic or nonbiodegradable fluorescent probes commonly employed for *in vivo* imaging.[24,32,46,60,62,63]

The advantage of time-gated imaging in general, and of its application to silicon nanoparticles embodied in the GLISiN method of this work, lies in the superior sensitivity with regard to suppressing tissue autofluorescence. A particular challenge in translation of theranostic nanomaterials to the clinic is the drive to minimize the amount of material in an injected dose. The ability of the method to more reliably identify and track the nanoconstructs, and the lower toxicity exhibited by the silicon-based quantum dots used, provides a promising path for *in vivo* imaging both in the research lab and in the clinic.

MATERIALS AND METHODS

Preparation of PSiNPs

Luminescent porous silicon nanoparticles (PSiNPs) were prepared by electrochemical perforation etching of silicon wafers, as described previously.[50] Briefly, highly boron-doped

p^{++}-type silicon wafers (~1 mΩ-cm resistivity, Virginia Semiconductor, Inc.) were anodically etched in an electrolyte composed of 3:1 (v:v) of 48% aqueous HF:ethanol. The etching waveform consisted of a square wave in which a lower current density of 50 mA cm^{-2} was applied for 1.8 s, followed by a higher current density pulse of 400 mA cm^{-2} applied for 0.36 s. This waveform was repeated for 140 cycles, generating a stratified porous silicon film with alternating layers of high and low porosity. The resulting porous silicon films were removed from the silicon substrate by applying a current density of 3.7 mA cm^{-2} for 250 s in a solution containing 1:20 (v:v) of 48% aqueous HF:ethanol. The freestanding porous silicon film was fractured by ultrasonication for 16 h, and the resulting nanoparticles were mildly oxidized by immersion in aqueous solution of sodium tetraborate (0.8 mM) to activate photo-luminescence.[51] To conjugate peptides to the PSiNPs, a 500 μL aliquot of PSiNPs (2 mg mL^{-1} in ethanol) was mixed with 10 μL of 3-(ethoxydimethyl)-propylamine silane by vortex overnight. The nanoparticles were rinsed three times with ethanol and then further reacted with 500 μL of succinimidyl carboxy methyl ester–polyethylene glycol–maleimide (SCM-PEG-MAL, MW 5000, Laysan Bio, 10 mg mL^{-1} in ethanol) for 2 h, followed by rinsing with ethanol and deionized water. Finally, the nano-particles were reacted with iRGD (500 μL, 1 mg mL^{-1}) by vortex for 2 h to conjugate the peptide via a free cysteine residue on iRGD.[64] Conjugation was confirmed by measuring fluorescence of a FAM tagged to the peptide, that is ~100 nmol mg^{-1} (peptide/PSiNPs). Control (nontargeted) PSiNPs for the *in vivo* administration experiments were prepared similarly but contained only the succinimidyl carboxy methyl ester–polyethylene glycol surface chemistry (SCM-PEG, MW 5000, Laysan Bio) with no pendant peptide.

Characterization of PSiNPs

Transmission electron microscope (TEM) images were obtained on a JEOL-1200 EX II operating at 120 kV (Supporting Information Figure S9a). Dynamic light scattering (DLS, Zetasizer ZS 90, Malvern Instruments) was used to determine the hydrodynamic size and zeta potential of the nanoparticles (Supporting Information Figure S9b). Steady-state photoluminescence/fluorescence spectra (λ_{ex} = 365 nm) were obtained using a QE pro spectrometer (Ocean Optics) fitted with a 460 nm long-pass emission filter (Supporting Information Figure S1).

Gated Luminescence Imaging of Silicon Nanoparticles (GLISiN)

A custom-built time-domain imaging system was used to acquire photoluminescence decay and time-gated images (Figure 1). One of two LED sources (λ_{ex} = 365 nm and λ_{ex} = 455 nm, Ocean Optics) or a tunable laser consisting of a tripled Nd:YAG-pumped optical parametric oscillator (Opolette 355, Opotek Inc.) were used as the excitation source at a repetition rate of 10 Hz, which was externally synchronized and triggered by a function generator (Keithley 3390 50 MHz arbitrary waveform generator). Time-resolved image and spectral data were obtained with an intensified CCD camera (iSTAR 334T, Andor Technology Ltd.). The Andor SOLIS software was used to program delays and timing pulses and to analyze images including signal-to-noise ratio (SNR). A full description of the SNR calculation and GLISiN operating conditions is available in Supporting Information Notes S1 and S2. For *in vitro* comparison, each aliquot of PSiNPs (100 μg mL^{-1}) and Alexa Fluor 647 (AF647, 1.5 μg mL^{-1}) was placed in separate cuvettes next to each other and imaged at

the same time with the GLISiN system (Supporting Information Figure S1). For the *ex vivo* mouse tissue images, each tissue was placed on a black polystyrene plate. The phantom samples consisted of 5 μL aliquots of PSiNPs or AF647 spotted on the plate next to the tissue of interest and imaged simultaneously. For the tissue imaging study, the organs were collected from female BALB/c mice bearing 4T1 breast tumor xenografts. Intensity scales for all the GLISiN images presented are set to encompass the minimum and maximum intensity measured in the respective image, *i.e.*, data were not excluded based on minimum or maximum intensity thresholds.

In Vivo Tumor Targeting Study

All studies in mice were approved by the Sanford-Burnham Medical Research Institute Committee on Animal Use and Care. BALB/c mice were purchased from Harlan Laboratories. 4T1 mouse breast tumor cells were cultured as recommended by the American Type Culture Collection and injected into BALB/c mice to establish xenograft tumors and grown to ~8 mm. PSiNPs and PSiNPs–iRGD dispersed in aqueous phosphate buffered saline (PBS) were administered through retro-orbital injection to mice (10 mg kg^{-1}). After 4 h of circulation, the mice were sacrificed and the major organs were harvested. Fluorescence images of the organs were acquired using a conventional animal imaging system (IVIS 200, Xenogen) and the imaging system described in this work (CWI and GLISiN).

Statistical Analysis

All data represent mean values ± standard deviation obtained from four mice per each group. Statistical significance was evaluated using two-tailed heteroscedastic Student's *t* test. The tumor accumulation difference between PSiNPs and PSiNP–iRGD was considered statistically significant with probability $p < 0.005$.

Supplementary Material

Refer to Web version on PubMed Central for supplementary material.

Acknowledgment

REFERENCES AND NOTES

1. Fernandez-Suarez M, Ting AY. Fluorescent Probes for Super-Resolution Imaging in Living Cells. Nature Rev. Mol. Cell Biol. 2008; 9:929–943. [PubMed: 19002208]

2. Giepmans BNG, Adams SR, Ellisman MH, Tsien RY. Review—The Fluorescent Toolbox for Assessing Protein Location and Function. Science. 2006; 312:217–224. [PubMed: 16614209]

3. Kobayashi H, Ogawa M, Alford R, Choyke PL, Urano Y. New Strategies for Fluorescent Probe Design in Medical Diagnostic Imaging. Chem. Rev. 2010; 110:2620–2640. [PubMed: 20000749]

4. Shcherbakova DM, Verkhusha VV. Near-Infrared Fluorescent Proteins for Multicolor *in vivo* Imaging. Nature Methods. 2013; 10:751–754. [PubMed: 23770755]

5. So MK, Xu CJ, Loening AM, Gambhir SS, Rao JH. Self-illuminating Quantum Dot Conjugates for *in vivo* Imaging. Nature Biotechnol. 2006; 24:339–343. [PubMed: 16501578]

6. Xiong LQ, Shuhendler AJ, Rao JH. Self-luminescing BRET-FRET Near-infrared Dots for *in vivo* Lymph-Node Mapping and Tumour Imaging. Nature Commun. 2012; 3:1193. [PubMed: 23149738]

7. Park J, Estrada A, Sharp K, Sang K, Schwartz JA, Smith DK, Coleman C, Payne JD, Korgel BA, Dunn AK, Tunnell JW. Two-Photon-Induced Photoluminescence Imaging of Tumors Using Near-Infrared Excited Gold Nanoshells. Opt. Express. 2008; 16:1590–1599. [PubMed: 18542237]

8. Yong KT, Qian J, Roy I, Lee HH, Bergey EJ, Tramposch KM, He SL, Swihart MT, Maitra A, Prasad PN. Quantum Rod Bioconjugates as Targeted Probes for Confocal and Two-Photon Fluorescence Imaging of Cancer Cells. Nano Lett. 2007; 7:761–765. [PubMed: 17288490]

9. Wang HF, Huff TB, Zweifel DA, He W, Low PS, Wei A, Cheng JX. *In Vitro* and *in Vivo* Two-Photon Luminescence Imaging of Single Gold Nanorods. Proc. Natl. Acad. Sci. U. S. A. 2005; 102:15752–15756. [PubMed: 16239346]

10. Liu S, Chen GY, Ohulchanskyy TY, Swihart MT, Prasad PN. Facile Synthesis and Potential Bioimaging Applications of Hybrid Upconverting and Plasmonic $NaGdF_4$: Yb^{3+}, Er^{3+}/Silica/Gold Nanoparticles. Theranostics. 2013; 3:275–281. [PubMed: 23606914]

11. Li M, Selvin PR. Luminescent Polyaminocarboxylate Chelates of Terbium and Europium: The Effect of Chelate Structure. J. Am. Chem. Soc. 1995; 117:8132–8138.

12. Zhang L, Zheng X, Deng W, Lu Y, Lechevallier S, Ye Z, Goldys EM, Dawes JM, Piper JA, Yuan J, Vereist M, Jin D. Practical Implementation, Characterization and Applications of a Multi-Colour Time-Gated Luminescence Microscope. Sci. Rep. 2014; 4:6597. [PubMed: 25307702]

13. Liu XY, Ye ZQ, Wei W, Du YG, Yuan JL, Ma D. Artificial Luminescent Protein as a Bioprobe for Time-Gated Luminescence Bioimaging. Chem. Commun. 2011; 47:8139–8141.

14. Song CH, Ye ZQ, Wang GL, Jin DY, Yuan JL, Guan YF, Piper J. Preparation and Time-Gated Luminescence Bioimaging Application of Ruthenium Complex Covalently Bound Silica Nanoparticles. Talanta. 2009; 79:103–108. [PubMed: 19376351]

15. Zhang J, Fu Y, Lakowicz JR. Fluorescent Metal Nano-shells: Lifetime-Tunable Molecular Probes in Fluorescent Cell Imaging. J. Phys. Chem. C. 2011; 115:7255–7260.

16. Dahan M, Laurence T, Pinaud F, Chemla DS, Alivisatos AP, Sauer M, Weiss S. Time-Gated Biological Imaging by Use of Colloidal Quantum Dots. Opt. Lett. 2001; 26:825–827. [PubMed: 18040463]

17. Yong KT, Wang YC, Roy I, Rui H, Swihart MT, Law WC, Kwak SK, Ye L, Liu JW, Mahajan SD, Reynolds JL. Preparation of Quantum Dot/Drug Nanoparticle Formulations for Traceable Targeted Delivery and Therapy. Theranostics. 2012; 2:681–694. [PubMed: 22896770]

18. Beeby A, Botchway SW, Clarkson IM, Faulkner S, Parker AW, Parker D, Williams JAG. Luminescence Imaging Microscopy and Lifetime Mapping Using Kinetically Stable Lanthanide(III) Complexes. J. Photochem. Photobiol., B. 2000; 57:83–89. [PubMed: 11154087]

19. Thibon A, Pierre VC. Principles of Responsive Lanthanide-Based Luminescent Probes for Cellular Imaging. Anal. Bioanal. Chem. 2009; 394:107–120. [PubMed: 19283368]

20. Vicidomini G, Moneron G, Han KY, Westphal V, Ta H, Reuss M, Engelhardt J, Eggeling C, Hell SW. Sharper Low-Power STED Nanoscopy by Time Gating. Nature Methods. 2011; 8:571–U75. [PubMed: 21642963]

21. Cheng X, Lowe SB, Reece PJ, Gooding JJ. Colloidal Silicon Quantum Dots: From Preparation To The Modification Of Self-Assembled Monolayers (Sams) For Bio-Applications. Chem. Soc. Rev. 2014; 43:2680–2700. [PubMed: 24395024]

22. Yong KT, Law WC, Hu R, Ye L, Liu LW, Swihart MT, Prasad PN. Nanotoxicity Assessment Of Quantum Dots: From Cellular To Primate Studies. Chem. Soc. Rev. 2013; 42:1236–1250. [PubMed: 23175134]

23. Liu JW, Erogbogbo F, Yong KT, Ye L, Liu J, Hu R, Chen HY, Hu YZ, Yang Y, Yang JH, Roy I, Karker NA, Swihart MT, Prasad PN. Assessing Clinical Prospects of Silicon Quantum Dots: Studies in Mice and Monkeys. ACS Nano. 2013; 7:7303–7310. [PubMed: 23841561]

24. Gu L, Hall DJ, Qin ZT, Anglin E, Joo J, Mooney DJ, Howell SB, Sailor MJ. *In Vivo* Time-Gated Fluorescence Imaging with Biodegradable Luminescent Porous Silicon Nanoparticles. Nature Commun. 2013; 4:2326. [PubMed: 23933660]

25. Erogbogbo F, Liu X, May JL, Narain A, Gladding P, Swihart MT, Prasad PN. Plasmonic Gold and Luminescent Silicon Nanoplatforms for Multimode Imaging of Cancer Cells. Integr. Biol. 2013; 5:144–150.

26. Erogbogbo F, Chang CW, May JL, Liu LW, Kumar R, Law WC, Ding H, Yong KT, Roy I, Sheshadri M, Swihart MT, Prasad PN. Bioconjugation of Luminescent Silicon Quantum Dots to Gadolinium Ions for Bioimaging Applications. Nanoscale. 2012; 4:5483–5489. [PubMed: 22854899]

27. Erogbogbo F, Chang CW, May J, Prasad PN, Swihart MT. Energy Transfer from a Dye Donor to Enhance the Luminescence of Silicon Quantum Dots. Nanoscale. 2012; 4:5163–5168. [PubMed: 22802158]

28. Cheng X, Gondosiswanto R, Ciampi S, Reece PJ, Gooding JJ. One-Pot Synthesis of Colloidal Silicon Quantum Dots and Surface Functionalization via Thiol-Ene Click Chemistry. Chem. Commun. 2012; 48:11874–11876.

29. Lockwood R, McFarlane S, Nunez JRR, Wang XY, Veinot JGC, Meldrum A. Photoactivation of Silicon Quantum Dots. J. Lumin. 2011; 131:1530–1535.

30. Erogbogbo F, Tien CA, Chang CW, Yong KT, Law WC, Ding H, Roy I, Swihart MT, Prasad PN. Bioconjugation of Luminescent Silicon Quantum Dots for Selective Uptake by Cancer Cells. Bioconjugate Chem. 2011; 22:1081–1088.

31. Kelly JA, Henderson EJ, Veinot JGC. Sol—Gel Precursors for Group 14 Nanocrystals. Chem. Commun. 2010; 46:8704–8718.

32. Park J-H, Gu L, Maltzahn G. v. Ruoslahti E, Bhatia SN, Sailor MJ. Biodegradable Luminescent Porous Silicon Nanoparticles for *in Vivo* Applications. Nature Mater. 2009; 8:331–336. [PubMed: 19234444]

33. Zou J, Kauzlarich SM. Functionalization of Silicon Nanoparticles *via* Silanization: Alkyl, Halide and Ester. J. Cluster Sci. 2008; 19:341–355.

34. Liu SM. Luminescent Silicon Nanoparticles Formed in Solution. J. Nanosci. Nanotechnol. 2008; 8:1110–1125. [PubMed: 18468111]

35. Erogbogbo F, Yong KT, Roy I, Xu GX, Prasad PN, Swihart MT. Biocompatible Luminescent Silicon Quantum Dots for Imaging of Cancer Cells. ACS Nano. 2008; 2:873–878. [PubMed: 19206483]

36. Zou J, Sanelle P, Pettigrew KA, Kauzlarich SM. Size and Spectroscopy of Silicon Nanoparticles Prepared *via* Reduction of $SiCl_4$. J. Cluster Sci. 2006; 17:565–578.

37. Veinot JGC. Synthesis, Surface Functionalization, and Properties of Freestanding Silicon Nanocrystals. Chem. Commun. 2006:4160–4168.

38. Derfus AM, Chan WCW, Bhatia SN. Probing the Cytotoxicity of Semiconductor Quantum Dots. Nano Lett. 2004; 4:11–18.

39. Cheng X, Lowe SB, Ciampi S, Magenau A, Gaus K, Reece PJ, Gooding JJ. Versatile "Click Chemistry" Approach to Functionalizing Silicon Quantum Dots: Applications toward Fluorescent Cellular Imaging. Langmuir. 2014; 30:5209–5216. [PubMed: 24716818]

40. Pan G-H, Barras A, Boussekey L, Qu X, Boukherroub R. Photochemical Reaction of Vitamin C with Silicon Nanocrystals: Polymerization, Hydrolysis and Photoluminescence. J. Mater. Chem. C. 2013; 1:5856–5865.

41. Sa'ar A. Photoluminescence from Silicon Nanostructures: The Mutual Role of Quantum Confinement and Surface Chemistry. J. Nanophotonics. 2009; 3:032501.

42. Salonen J, Kaukonen AM, Hirvonen J, Lehto VP. Mesoporous Silicon in Drug Delivery Applications. J. Pharm. Sci. 2008; 97:632–653. [PubMed: 17546667]

43. Anglin EJ, Cheng L, Freeman WR, Sailor MJ. Porous Silicon in Drug Delivery Devices and Materials. Adv. Drug Delivery Rev. 2008; 60:1266–1277.

44. Coffer JL, Montchamp JL, Aimone JB, Weis RP. Routes to Calcified Porous Silicon: Implications for Drug Delivery and Biosensing. Phys. Status Solidi A. 2003; 197:336–339.

45. Granitzer P, Rumpf K, Roca AG, Morales MP, Poelt P, Albu M. Magnetite Nanoparticles Embedded in Biodegradable Porous Silicon. J. Magn. Magnetic Mater. 2010; 322:1343–1346.

46. Kinsella JM, Ananda S, Andrew JS, Grondek JF, Chien MP, Scadeng M, Gianneschi NC, Ruoslahti E, Sailor MJ. Enhanced Magnetic Resonance Contrast of Fe_3O_4 Nanoparticles Trapped in a Porous Silicon Nanoparticle Host. Adv. Mater. 2011; 23:H248. [PubMed: 21842475]

47. Tasciotti E, Liu XW, Bhavane R, Plant K, Leonard AD, Price BK, Cheng MMC, Decuzzi P, Tour JM, Robertson F, Ferrari M. Mesoporous Silicon Particles as a Multistage Delivery System for Imaging and Therapeutic Applications. Nature Nanotechnol. 2008; 3(3):151–157. [PubMed: 18654487]

48. Chiappini C, Tasciotti E, Fakhoury JR, Fine D, Pullan L, Wang YC, Fu LF, Liu XW, Ferrari M. Tailored Porous Silicon Microparticles: Fabrication and Properties. ChemPhysChem. 2010; 11:1029–1035. [PubMed: 20162656]

49. Gu L, Park J-H, Duong KH, Ruoslahti E, Sailor MJ. Magnetic Luminescent Porous Silicon Microparticles for Localized Delivery of Molecular Drug Payloads. Small. 2010; 6:2546–2552. [PubMed: 20814923]

50. Qin Z, Joo J, Gu L, Sailor MJ. Size Control of Porous Silicon Nanoparticles by Electrochemical Perforation Etching. Part. Part. Syst. Charact. 2014; 31:252–256.

51. Joo J, Cruz JF, Vijayakumar S, Grondek J, Sailor MJ. Photoluminescent Porous Si/SiO_2 Core/Shell Nanoparticles Prepared by Borate Oxidation. Adv. Funct. Mater. 2014; 24:5688–5694.

52. Teesalu T, Sugahara KN, Kotamraju VR, Ruoslahti E. C-End Rule Peptides Mediate Neuropilin-1-Dependent Cell, Vascular, and Tissue Penetration. Proc. Natl. Acad. Sci. U. S. A. 2009; 106:16157–16162. [PubMed: 19805273]

53. Sugahara KN, Teesalu T, Karmali PP, Kotamraju VR, Agemy L, Greenwald DR, Ruoslahti E. Coadministration of a Tumor-Penetrating Peptide Enhances the Efficacy of Cancer Drugs. Science. 2010; 328:1031–1035. [PubMed: 20378772]

54. Lin ZJ, Alexandrakis G, Patel N, Shen JH, Tang LP, Liu HL. Time-Gated Optical Imaging to Detect Positive Prostate Cancer Margins. Proc. SPIE. 2009; 7161 71611910.1117/12.807886.

55. Cubeddu R, Canti G, Taroni P, Valentini G. Time-Gated Fluorescence Imaging for the Diagnosis of Tumors in a Murine Model. Photochem. Photobiol. 1993; 57(3):480–485. [PubMed: 8475182]

56. Patel NL, Lin Z-J, Rathore Y, Livingston EH, Liu H, Alexandrakis G. Relative Capacities of Time-Gated *versus* Continuous-Wave Imaging To Localize Tissue Embedded Vessels with Increasing Depth. J. Biomed. Opt. 2010; 15:016015. [PubMed: 20210461]

57. Iyer AK, Khaled G, Fang J, Maeda H. Exploiting the Enhanced Permeability and Retention Effect for Tumor Targeting. Drug Discovery Today. 2006; 11:812–818. [PubMed: 16935749]

58. Sugahara KN, Teesalu T, Karmali PP, Kotamraju VR, Agemy L, Girard OM, Hanahan D, Mattrey RF, Ruoslahti E. Tissue-Penetrating Delivery of Compounds and Nanoparticles into Tumors. Cancer Cell. 2009; 16:510–520. [PubMed: 19962669]

59. Cai WB, Shin DW, Chen K, Gheysens O, Cao QZ, Wang SX, Gambhir SS, Chen XY. Peptide-Labeled Near-Infrared Quantum Dots For Imaging Tumor Vasculature in Living Subjects. Nano Lett. 2006; 6:669–676. [PubMed: 16608262]

60. Gu L, Ruff LE, Qin ZT, Corr M, Hedrick SM, Sailor MJ. Multivalent Porous Silicon Nanoparticles Enhance the Immune Activation Potency of Agonistic CD40 Antibody. Adv. Mater. 2012; 24:3981–3987. [PubMed: 22689074]

61. Canham LT. Bioactive Silicon Structure Fabrication Through Nanoetching Techniques. Adv. Mater. 1995; 7:1033–1037.

62. Secret E, Maynadier M, Gallud A, Chaix A, Bouffard E, Gary-Bobo M, Marcotte N, Mongin O, El Cheikh K, Hugues V, Auffan M, Frochot C, Morere A, Maillard P, Blanchard-Desce M, Sailor MJ, Garcia M, Durand J-O, Cunin F. Two-Photon Excitation of Porphyrin-Functionalized Porous Silicon Nanoparticles for Photodynamic Therapy. Adv. Mater. 2014; 26:7643–7648. [PubMed: 25323443]

63. Xiao L, Gu L, Howell SB, Sailor MJ. Porous Silicon Nanoparticle Photosensitizers for Singlet Oxygen and Their Phototoxicity against Cancer Cells. ACS Nano. 2011; 5:3651–3659. [PubMed: 21452822]

64. Cai WB, Chen XY. Preparation of Peptide-Conjugated Quantum Dots for Tumor Vasculature-Targeted Imaging. Nature Protoc. 2008; 3:89–96. [PubMed: 18193025]
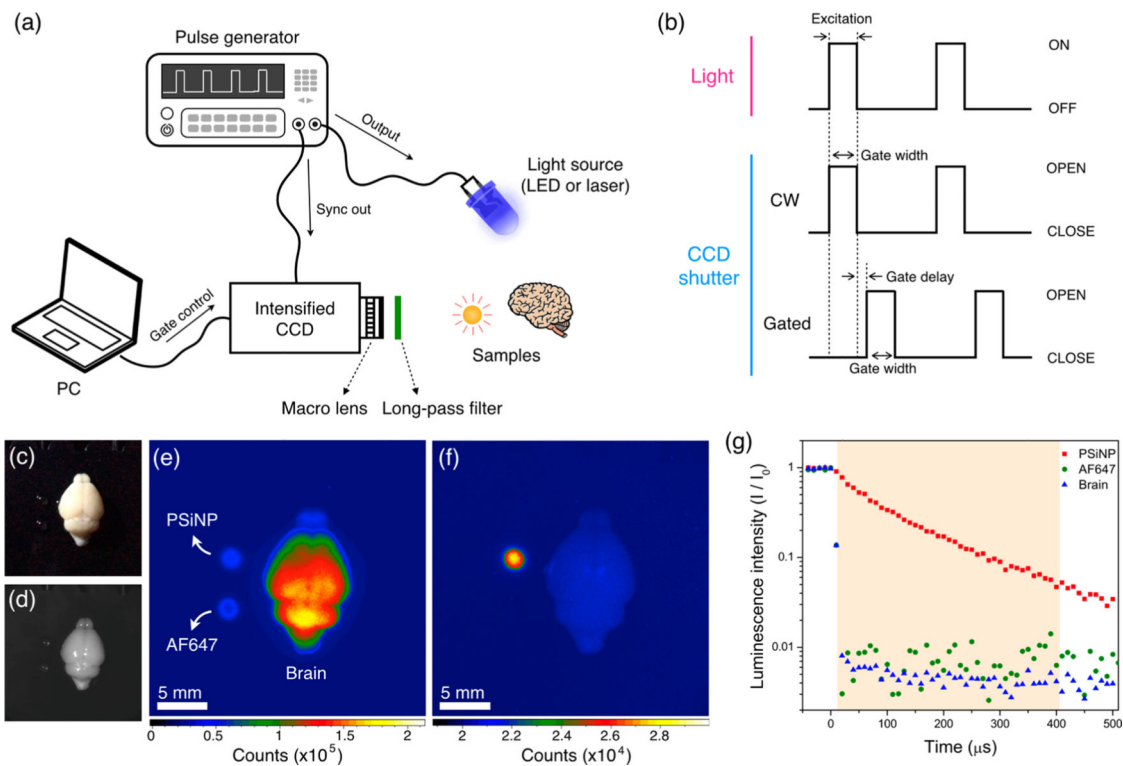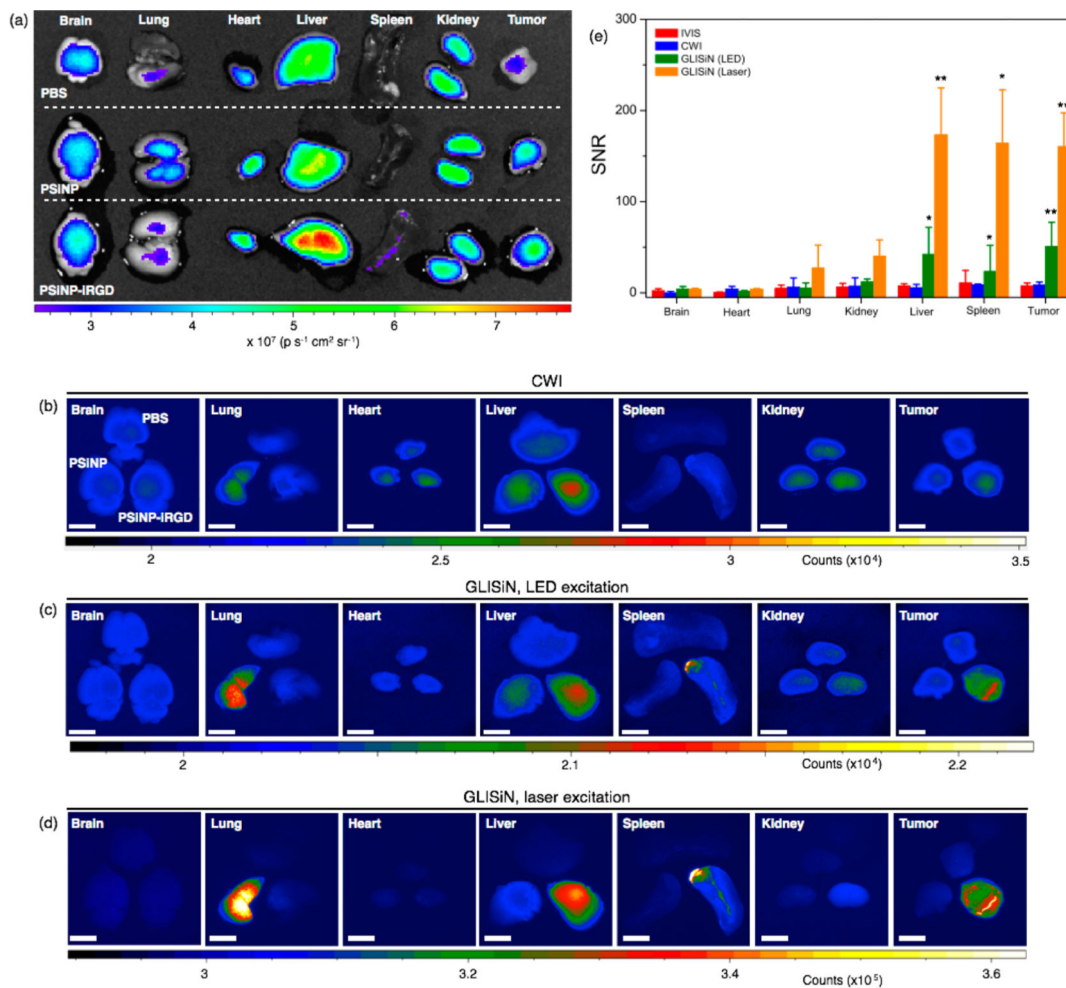
Figure 1.
Methodology and example of data obtained for gated luminescence imaging of Si nanoparticles (GLISiN) compared with steady-state imaging. (a) Schematic showing the instrumental setup. The iCCD camera and the light source were controlled by an external pulse generator. In the case of laser illumination, the laser fired under control of the laser's internal pulse generator, and the camera was configured to slave to it via TTL trigger. (b) Notional waveforms for illumination and camera gating used to acquire images. LED was triggered "ON" by the pulse generator, maintained in the "ON" position for the duration of "Gate width", and then image acquisition terminated ("CLOSE") at the end of the "Gate width" period. For the laser experiments, the laser fired at the beginning of "Gate width" but was only "ON" for the duration of the natural pulse width of the laser (~8 ns). For GLISiN imaging ("Gated"), the camera was preprogrammed to energize the intensifier screen ("OPEN") at a time delayed by "Gate delay" relative to the end of the excitation pulse. For continuous wave ("CW") imaging, the camera was again programmed to be "OPEN" for the "Gate width" period, but the "Gate width" period overlapped with the laser or LED excitation pulse, generating a pseudo steady-state measurement. (c) Digital color photograph (from iPhone 5, Apple Inc.) and (d) gray scale image (from Andor iCCD) of mouse brain obtained under ambient light. (e) CW and (f) GLISiN images of the same brain under UV LED excitation (λ_{ex}= 365 nm, λ_{em}= 460 nm long-pass filter; gate width, 400 μs, 40 accumulations, gate delay for CW = 0 μs, gate delay for GLISiN = 5 μs). Phantom samples corresponding to 150 ng of porous Si nanoparticles ("PSiNP") and 2.5 ng of the molecular dye Alexa Fluor 647 ("AF647") were dropped next to the brain for comparison, as indicated. Note that the signals from the AF647 sample (fluorescence) and the brain tissue (autofluorescence), readily visible at steady state (e), almost disappear in the GLISiN image

(f), whereas the longer-lived luminescence from PSiNP is much stronger in the GLISiN image. (g) Normalized intensity decay of the photoluminescence/fluorescence signals from the samples in (c–f) as a function of time after excitation pulse (gate width, 10 μs; gate step increase, 10 μs; accumulation, 20 times). Note the nanosecond decay times of the organic dye and tissue autofluorescence are too short to be resolved at the measurement time scale. The orange box depicts the "Gate width" window used to obtain GLISiN images in (f).
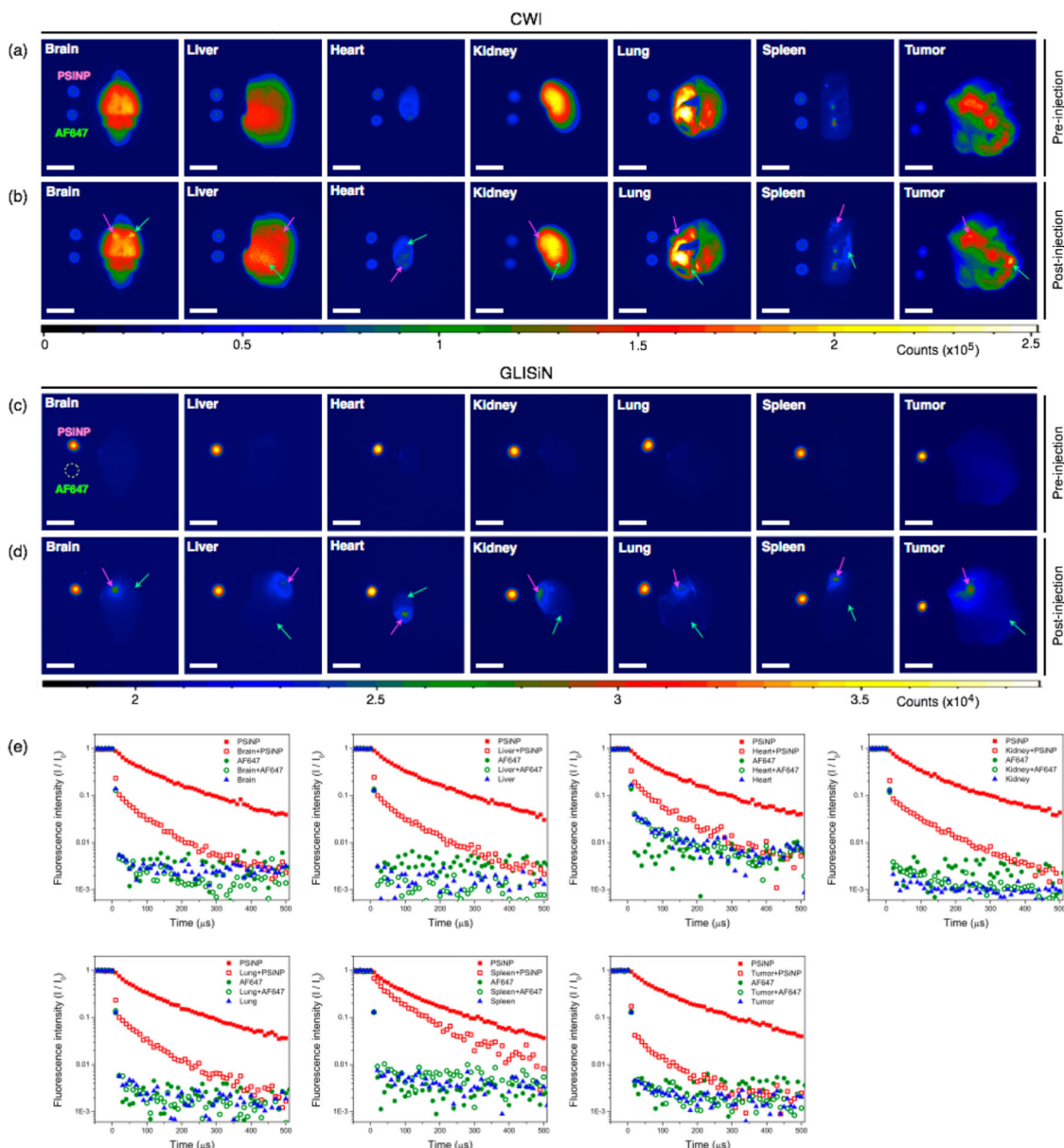
Figure 2.
Comparison of fluorescence and time-gated luminescence images of mouse tissues before and after localized injection of porous Si nanoparticles (PSiNPs) and the molecular dye (AF647). (a) CW images of organs (as indicated) harvested from a 4T1 breast tumor-bearing BALB/c mouse before local injection of imaging agents. Aliquots (5 μL) of the PSiNP (100 μg/mL, corresponding to 500 ng) and AF647 (1.5 μg/mL, corresponding to 7.5 ng) imaging agents are spotted to the left of each tissue for comparison. (b) CW images of the same organs, after local injection of PSiNP (200 ng) and AF647 (3 ng) in the locations indicated by pink and green arrows, respectively. Both imaging agents are difficult to discern against tissue autofluorescence. (c) GLISiN images of the same organs before injection of imaging agents, as in (a). (d) GLISiN images of the same organs after injection of imaging agents, as in (b). Scale bar: 5 mm. Samples were not moved between CW and GLISiN image

acquisition. (e) Normalized intensity of the photoluminescence/fluorescence signals as a function of time after excitation pulse. Red solid squares, PSiNPs in the phantom image (spotted adjacent to each organ); red open squares, PSiNP-injected tissue region; green solid circles, AF647 in the phantom image (spotted adjacent to each organ); green open circles, AF647-injected tissue region; blue solid triangles, tissue control (away from region of either injection). Optical setup, long-pass filter, excitation source (365 nm UV LED) and gating parameters the same as in Figure 1.

Figure 3.

Comparison of fluorescence and time-gated luminescence images of tissues harvested from mice with breast tumors. Live mice were injected with untargeted PSiNPs, iRGD-targeted PSiNPs, or phosphate buffered-saline (PBS), and then sacrificed 4 h postinjection. (a) Conventional IVIS image (λ_{ex}= 445–490 nm, GFP filter, λ_{em}= 695–770 nm, Cy5.5 filter). (b–d) Organs from three separate animals in the same image, each injected with one of the three formulations (PBS, PSiNP, and PSiNP–iRGD, as indicated). (b) CW image (λ_{ex}= 455 nm, λ_{em}= 700 nm long-pass filter), (c) GLISiN image obtained with pulsed UV LED excitation (λ_{ex}= 365 nm, λ_{em}= 460 nm long-pass filter), and (d) GLISiN image obtained with pulsed laser excitation (λ_{ex}= 455 nm, λ_{em}= 700 nm long-pass filter). Scale bar = 5 mm. (e) Signal-to-noise ratio (SNR) calculated for the targeted nanoparticles (PSiNP–iRGD) for each imaging method, quantified per organ. The SNR is calculated relative to the PBS-injected mouse tissues. Red, IVIS image; blue, CW image; green, GLISiN (with LED excitation); orange, GLISiN (with laser excitation).